Electronic Supplementary Information (ESI)

Bio-inspired 3D Quasi-fractal Nanostructure for Improved Oxygen Evolution Reaction

Wei Wei,[a] Weidong He,[a] Bibo Shi,[a] Guanping Dong,[ab] Xubing Lu,[a] Min Zeng,[a] Xingsen Gao,[a] Qianming Wang,[c] Guofu Zhou,[d] Jun-Ming Liu,[ae] Andrzej Herczynski,[f] Krzysztof Kempa[af] and Jinwei Gao*[a]

[a]Institute for Advanced Materials, South China Academy of Advanced Optoelectronics and Guangdong Provincial Laboratory of Quantum Engineering and Quantum Materials, South China Normal University, Guangzhou, 510006, China.

[b]School of Mechanical and Automotive Engineering, South China University of Technology, Guangzhou 510640, China

[c]School of Chemistry & Environment, South China Normal University, Guangzhou 510006, China.

[d]Electronic Paper Displays Institute, South China Academy of Advanced Optoelectronics, South China Normal University, Guangzhou, 510006, China

[e]Laboratory of Solid State Microstructures, Innovation Center of Advanced Microstructures, Nanjing University, Nanjing 210093, China

[f]Department of Physics, Boston College, Chestnut Hill, Massachusetts 02467, USA

Corresponding author: gaojinwei@m.scnu.edu.cn

CONTENTS

1. Experimental Section

2. Supplementary Figures

3. Supplementary Tables

1. Experimental Section

Materials. All chemicals were used as received without further purification. Nickel chloride hexahydrate ($NiCl_2 \cdot 6H_2O$, AR), Sodium chloride (NaCl, AR), ammonium chloride (NH_4Cl, AR), Ethylene glycol $(CH_2OH)_2$, AR), and ferrous sulfate ($FeSO_4 \cdot 7H_2O$, AR) were purchased from Shanghai Hushi Chemical Reagent Factory. NF (nickel foam, ~0.5m^2/g) was purchased from Shanxi Lizhiyuan Electronics Co.Ltd.

Synthesis of DNT/NF. Prior to electrodeposition, a piece of NF (1cm*1cm, ~0.3g) was cleaned with 3M HCl, acetone and deionized water through ultrasonic cleaning in sequence. After the Nitrogen blowing, the NF and Pt wire were used as the working electrode and counter electrode respectively, under a constant current of ~1.0 A cm^{-2} for 180 s in a beaker with 40 ml deionized water, 0.1M $NICl_2 \cdot 6H_2O$, 0.5M NH_4Cl and 2M NaCl to obtain the dendritic nickel tree nanostructure.

Synthesis of $Ni(OH)_2$/DNT. The DNT was sealed into a Teflon-lined stainless-steel autoclave of 25ml containing 15ml deionized water and maintained ~150°C for 5 h. To the best of our knowledge, the synthesis of $Ni(OH)_2$ nanosheets with H_2O only is the first time. The mechanism is as following：

$$Ni + n\,H_2O \rightarrow [Ni(H_2O)_n]^{2+} + 2e^-$$

$$O_2 + 2H_2O + 4e^- \rightarrow 4OH^-$$

$$[Ni(H_2O)_n]^{2+} + 2OH^- \rightarrow Ni(OH)_2 + nH_2O$$

Synthesis of Fe/Ni(OH)$_2$/DNT. Under the protection of N_2, the 30 ml Ethylene glycol and 5 mmol $FeSO_4 \cdot 7H_2O$ were mixed together and stirred for 30 min. Then, the Ni(OH)$_2$/DNT was immersed in the solution and transferred into a 50 mL Teflon-lined stainless-steel autoclave, maintained about 15h under 240°C. After cooling to room temperature naturally, the sample was washed 3 times with DI water and alcohol respectively, then dried at 80℃ in a vacuum oven overnight.

Structure characterizations. X-ray diffraction (XRD) patterns were collected on a PANalytical X Pert Powder diffractometer with Ni Kα radiation. The chemical elements were catalogued by an X-ray photoelectron spectroscopy (XPS) with ESCALAB 250 Xi. The morphologies of the catalysts were observed using a field-emission scanning electron microscopy (SEM, Carry Scope JCM-5700) at accelerating voltage of 20 kV. The transmission electron microscopy (TEM) images were obtained on a JEM-2100HR, while Energy Dispersive X-Ray (EDX) mappings were acquired on an Oxford instrument IET250 spectrometer.

Electrochemical Measurements. The electrocatalytic properties of the products for OER were evaluated with a three electrode system using a CHI electrochemical workstation (model 660E). The as-prepared composite was employed as the working electrode**.** A standard Hg/HgO electrode and a graphite rod were used as the reference

and counter electrodes, respectively. All tests were carried out in O_2-saturated solution of 1 M KOH. All potentials were measured relative to the reversible hydrogen electrode (RHE), and the potential drop resulted from the ohmic loss on the electrolyte resistance has been subtracted. All potentials were referenced to the reversible hydrogen electrode (RHE) through calibration: E (RHE) = E (Hg/HgO) + 0.098 + 0.059 × pH. Linear sweep voltammetry (LSV) was conducted at a scan rate of 2 mV s^{-1}. Stability measurement was performed using chronopotentiometry. Electrochemical impedance spectroscopy (EIS) was carried out in potentiostatic mode from 10^5- 0.1 Hz with overpotential of 300mv. All the polarization curves are the steady-state ones after several cycles.

2. Supplementary Figures

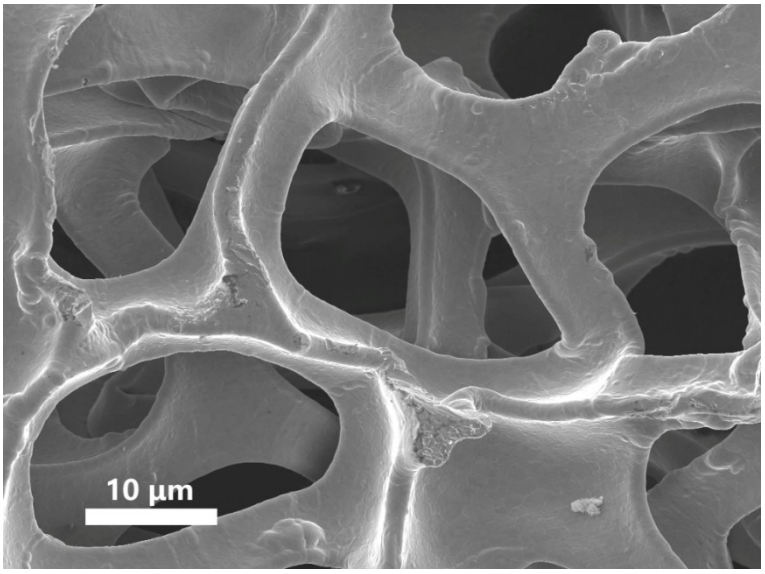

Supplementary Figure 1. SEM image of a typical bare nickel foam

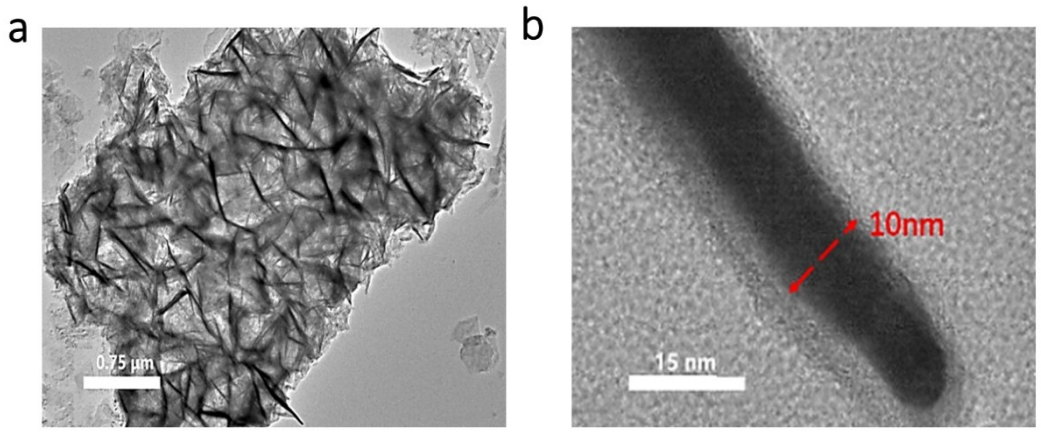

Supplementary Figure 2 (a) TEM and (b) HRTEM images of $Ni(OH)_2$ sheets.

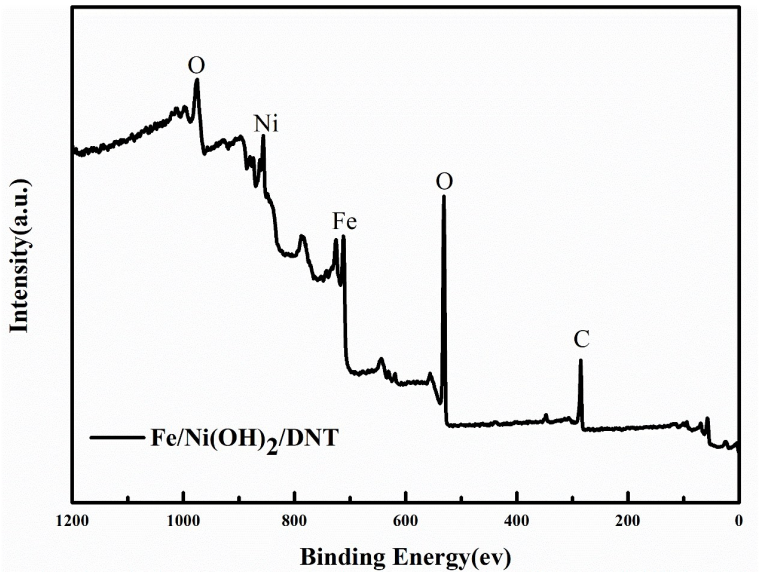

Supplementary Figure 3 The full spectrum of XPS spectra of $Fe/Ni(OH)_2/DNT$

The full spectrum of XPS spectra in Figure S3 demonstrates the presence of Ni, Fe, O elements in the composites. The high-resolution XPS spectra of Fe 2p and Ni 2p (Figure 2a, b) show that, two prominent peaks located at 711.5 eV and 725.3 eV, namely Fe 2p 3/2 and Fe 2p 1/2, indicating the Fe^{2+} oxidation state, shifts negatively. While two peaks located at binding energy of 856.0 eV, and 873.7 eV, along with two shakeup satellites, namely Ni 2p 1/2 and Ni 2p3/2 respectively, indicated that the Ni^{2+} condition exists. Compared with the criteria data established by Biesinger et.al[1], the position moves right and positively. When loading the positive potential, it would be easy to change into high valence Ni^{4+}, enhancing the performance. In addition, the high-resolution spectra of O1s (Figure 2c) elucidates the existence of double oxygen species denoted as O1s A

and O1s B, respectively. The fitting peak of O1s A at 530.1 eV is pointed to the oxygen–metal bond, the O1s located at 531.6 eV is commonly associated with oxygen from the hydroxyl groups, showing the existence of $Ni(OH)_2$, with all peaks shift positively. All these indicate the partial electrons transfer from Ni^{2+}, O^{2-} to Fe^{2+}.

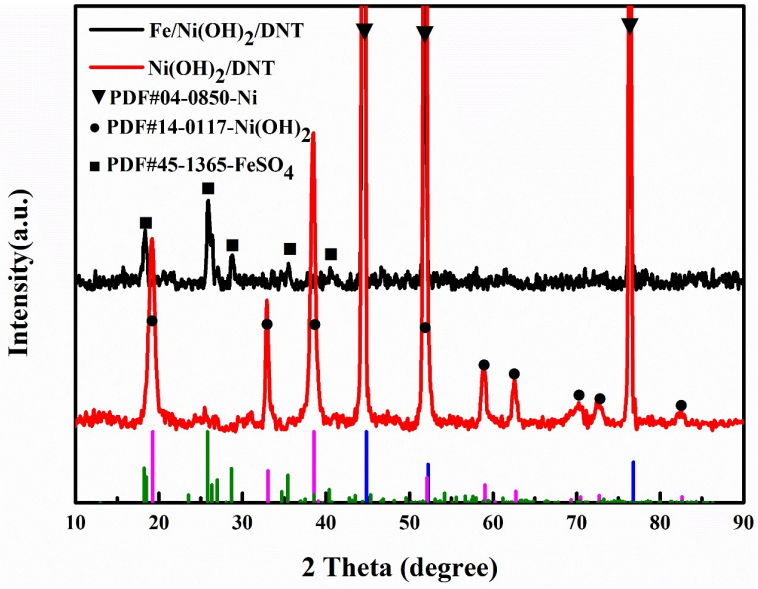

Supplementary Figure 4 XRD pattern of the $Ni(OH)_2$/DNT, and Fe/Ni $(OH)_2$/DNT

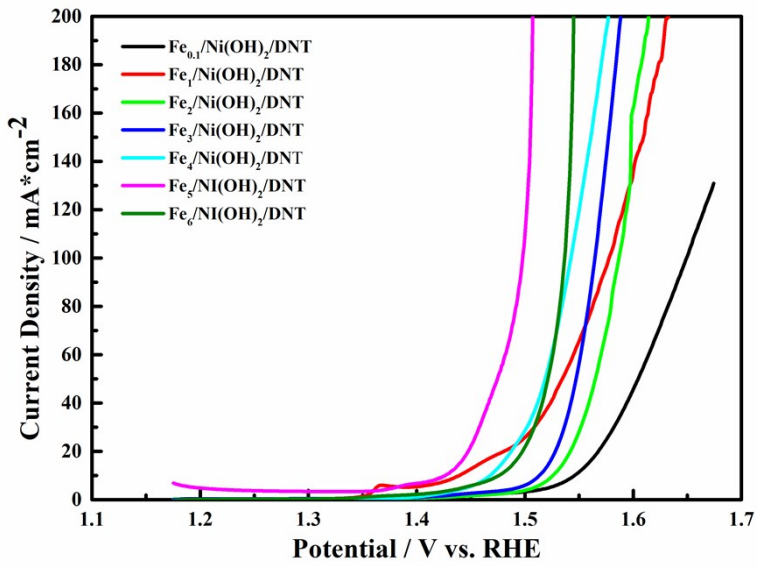

Supplementary Figure 5 Steady-state current densities as a function of the applied potential in 1 M KOH solution over as-prepared $Fe_x/Ni(OH)_2$/DNT , the x means the react concentration of Fe-ion in the hydrothermal reaction.

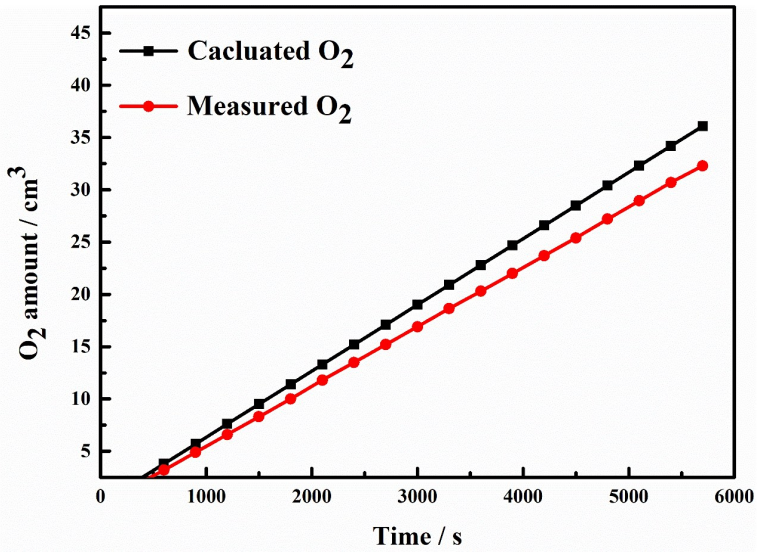

Supplementary Figure 6 Faraday test of the Fe/Ni(OH)$_2$/DNT

Comparison of the amount of O_2 that can be theoretically evolved by OER, which is calculated based on the Faradic law, and the amount of O_2 obtained experimentally generated by OER as catalyzed by Fe/Ni(OH)$_2$/DNT. The graphs are plotted as function of reaction time. The experimental value was derived from the CP curve at a current density of 100 mA cm^{-2}.

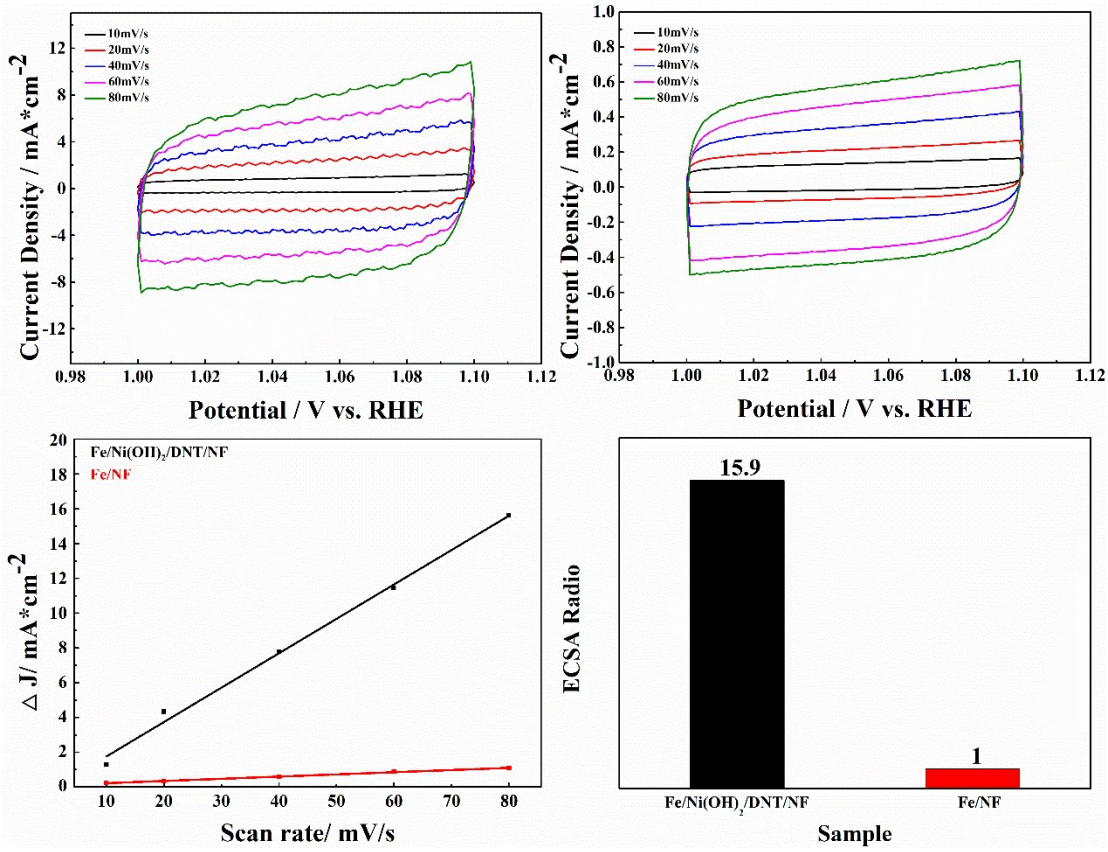

Supplementary Figure 7 (a) and (b) CV (cyclic voltammetry) for the Fe/Ni(OH)$_2$/DNT and Fe/NF systems, respectively. (c) The current density as a function of the Scan rates over the samples (d) the surface area ratio for Fe/Ni(OH)$_2$/DNT and Fe/NF systems.

To gain the corresponding electrochemical surface area (ECSA), double layer Capacitance (Cdl) of the materials was measured in 1 M KOH solution. Cyclic voltammetry scans of all the electrocatalysts were first performed in a large potential range of 1.0 to 1.8 V for 50 cycles to activate them. Then, scans with different scan rates (10, 20, 40, 60, 80 mV s^{-1}) were obtained in a potential window of 1.0 to 1.1 V, in which no Faradaic process occurred and the current emerged mainly from the double layer capacitance charging. The value of Cdl was then obtained from the linear curve of Δj [$(j_a - j_c)/2$] at 1.05 V (vs RHE) vs scan rate. That is widely accepted that the ECSA of a material with similar composition is proportional to its Cdl value, expected to be linearly proportional to the current density on the same voltage.

As shown in report[2], the specific capacitance of the sample or the capacitance of an atomically smooth planar surface of the material per unit area under identical electrolyte conditions is 40 μ F cm^{-2} in 1M KOH based on typical reported values.

Then, the electrochemical active surface area is calculated from the following formula:

$$A_{ECSA} = \frac{specfic\ capacitance}{40\ uF\ cm^{-2}\ per\ cm^{2}_{ECSA}}$$

Therefore, the actual surface area of the Fe/Ni$(OH)_2$/DNT sample with 1cm^2 geometric area in this manuscript was ~2462.5 cm^2 (98500/40), while the pristine Fe/NF was ~153.75 cm^2 (6150/40), which was similar to the data of Nickel foam above. The results show that the surface area has enhanced more than 15.9 times (2463/154). Due to the formation of multiple nanoarrays and mingled nanosheets, the nanostructure allows more effective accessibility of active sites, buffering the electrolyte and promoting gas diffusion, and resulting in much higher OER activity.

3. Supplementary Tables

Table S1: Comparison of the Catalytic Activity toward the OER in Alkaline Solution of the Fe/Ni$(OH)_2$/DNT with Other Reported High Performance OER Catalysts.

Catalyst	Electrolyte Solution	Current density (j) (mA/cm ^{2})	Overpotential at the corresponding j(mV)	Stability test(h)	Tafel (mV/dec)	Exchange current density (μA/cm^2)	Reference
Fe/Ni(OH)$_2$/DNT	1M KOH	10	227	~30	59	4.89	This Work
		100	263				
RuO$_2$	1M KOH	100	317	--	70	8.13	This Work
Fe-O$_2$ Cat	1M KOH	100	537	30	82.7	--	Reference[3]
NiFe-LDH	1M KOH	30	280	10	50	--	Reference [4]
NiFe-SW	1M KOH	10	240	24	38.9	--	Reference [5]
NiFe/NF	1M KOH	100	370	10	28	--	Reference [6]
(Ni–Fe) oxide nanotube array	0.1M KOH	5	380	4	142	--	Reference [7]
NiFeO$_x$/ITO	1M KOH	10	310	40	28	--	Reference [8]
NiFe LDH-NiSe/NF	1M KOH	100	240	12	65.6	--	Reference [9]
MoS$_2$-Ni$_3$S$_2$	1M KOH	10	249	50	57	--	Reference[10]
N-Ni$_3$S$_2$/NF	1M KOH	170	350	~3	70	--	Reference [11]
NiMoN/NF	1M KOH	100	343	30	101	--	Reference[12]
Ni-Fe-OH@Ni$_3$S$_2$/ NF	1M KOH	100	240	20	93	--	Reference[13]
Ni$_{0.9}$Fe$_{0.1}$/NF	1M KOH	10	330	~2	45	--	Reference[14]
Fe-Ni-Ox-NPs	1M KOH	10	286	--	38	--	Reference[15]
Ni$_{50}$Fe$_{50}$-DAT	1M KOH	100	300	72	--	--	Reference[16]
Ni−Fe films	1M KOH	20	280	--	~40	--	Reference[17]
Ni$_3$FeAl$_{0.91}$LDH	1M KOH	20	304	~18	57	--	Reference[18]
Exfoliated NiFe LDHs	1M KOH	10	300	13	40	--	Reference[19]
Ni-Fe LDH hollow prisms	1M KOH	10	280	~6	49.4	--	Reference[20]
NiSe–NiO$_x$/NF	1M KOH	15	274	40	128		Reference[21]
FeCoNiP	1M KOH	100	270	24	~70	--	Reference[22]
FeMnP/NF electrode	0.1M KOH	10	280	75	56	--	Reference[23]
NiSe$_2$	1M KOH	10	250	38	6	5.1	Reference[24]

Note: All these data about OER activities are in geometric activities, calculated by dividing the current density per geometric area.

Table S2: Benchmarking Parameters for Selected OER Catalysts Investigated in 1 M KOH

Catalyst	**ECSA/cm^2**	$j_{g,\ \eta=0.35\ V}$ /mA cm^{-2}	$j_{E,\ \eta=0.35\ V}$ /mA cm^{-2}	Reference
Fe/Ni(OH)$_2$/DNT	2462.5	2951	1.2	This work
Fe/NF	153.75	70	0.45	This work
NiFe	--	3.9	1.05	Reference[25]
RuO_2	--	17.5	0.09	Reference[25]
IrO_x	--	42	0.4	Reference[26]

Note: The ECSA (electrochemical active surface area) is calculated as above.

The geometric activity, and the corresponding ECSA activity (intrinsic activity), are shown in Table S2. The $j_{g,\ \eta=0.35\ V}$ (geometric activity) is calculated by dividing the current density per geometric area at the overpotential of 0.35 V based on the Tafel slope. The $j_{E,\ \eta=0.35\ V}$ (ECSA activity) is calculated by dividing the current density per ECSA at the overpotential of 0.35 V. Apparently, compared with typical catalysts, the ECSA activity (intrinsic activity) of Fe/Ni(OH)$_2$/DNT is better than the noble catalysts and the NiFe catalyst, implying the better performance.

Reference

1 M.C. Biesinger, B.P. Payne, L.W.M. Lau, A. Gerson, R.S.C. Smart, Surf. Interface Anal. 2009, 41, 324.

2 R. Gao, G. D. Li, J. Hu, Y. Wu, X. Lian, D. Wang and X. Zou, *Catal. Sci. Technol.*, 2016, **6**, 8268–8275.

3 X. Zou, Y. Wu, Y. Liu, D. Liu, W. Li, L. Gu, H. Liu, P. Wang, L. Sun and Y. Zhang, *Chem*, 2018, **4**, 1139–1152.

4 Z. Lu, W. Xu, W. Zhu, Q. Yang, X. Lei, J. Liu, Y. Li, X. Sun and X. Duan, *Chem. Commun.*, 2014, **50**, 6479–6482.

5 W. Zhang, Y. Wu, J. Qi, M. Chen and R. Cao, *Adv. Energy Mater.*, 2017, **7**.9，1602547-1602553.

6 H. Wang, H. W. Lee, Y. Deng, Z. Lu, P. C. Hsu, Y. Liu, D. Lin and Y. Cui, *Nat. Commun.*, 2015, **6**, 1–8.

7 Z. Zhao, H. Wu, H. He, X. Xu and Y. Jin, *J. Mater. Chem. A*, 2015, **3**, 7179–7186.

8 J. Wang, L. Ji and Z. Chen, *ACS Catal.*, 2016, **6**, 6987–6992.

9 S. Dutta, A. Indra, Y. Feng, T. Song and U. Paik, *ACS Appl. Mater. Interfaces*, 2017, **9**, 33766–33774.

10 Y. Yang, K. Zhang, H. Lin, X. Li, H. C. Chan, L. Yang and Q. Gao, *ACS Catal.*, 2017, **7**, 2357–2366.

11 P. Chen, T. Zhou, M. Zhang, Y. Tong, C. Zhong, N. Zhang, L. Zhang, C. Wu and Y. Xie, *Adv. Mater.*, 2017, **29**(30), 1701584 – 1701590.

12 P. Chen, T. Zhou, M. Zhang, Y. Tong, C. Zhong, N. Zhang, L. Zhang, C. Wu and Y. Xie, *Adv. Mater.*, 2017, **29**, 1701584–1701590.

13 X. Zou, Y. Liu, G. D. Li, Y. Wu, D. P. Liu, W. Li, H. W. Li, D. Wang, Y. Zhang and X. Zou, *Adv. Mater.*, 2017, **29**(22): 1700404 – 1700411.

14 X. Zhang, H. Xu, X. Li, Y. Li, T. Yang and Y. Liang, *ACS Catal.*, 2016, **6**, 580–588.

15 L. Wang, J. Geng, W. Wang, C. Yuan, L. Kuai and B. Geng, *Nano Res.*, 2015, **8**, 3815–3822.

16 T. T. H. Hoang and A. A. Gewirth, *ACS Catal.*, 2016, **6**, 1159–1164.

17 M. W. Louie and A. T. Bell, *J. Am. Chem. Soc.*, 2013, **135**, 12329–12337.

18 H. Liu, Y. Wang, X. Lu, Y. Hu, G. Zhu, R. Chen, L. Ma, H. Zhu, Z. Tie, J. Liu and Z. Jin, *Nano Energy*, 2017, **35**, 350–357.

19 F. Song and X. Hu, *Nat. Commun.*, 2014, **5**, 1–9.

20 L. Yu, J. F. Yang, B. Y. Guan, Y. Lu and X. W. D. Lou, *Angew. Chemie - Int. Ed.*, 2018, **57**, 172–176.

21 R. Gao, G. D. Li, J. Hu, Y. Wu, X. Lian, D. Wang and X. Zou, *Catal. Sci. Technol.*, 2016, **6**, 8268–8275.

22 J. Xu, J. Li, D. Xiong, B. Zhang, Y. Liu, K. H. Wu, I. Amorim, W. Li and L. Liu, *Chem. Sci.*, 2018, **9**, 3470–3476.

23 Z. Zhao, D. E. Schipper, A. P. Leitner, H. Thirumalai, J. H. Chen, L. Xie, F. Qin, M. K. Alam, L. C. Grabow, S. Chen, D. Wang, Z. Ren, Z. Wang, K. H. Whitmire and J. Bao, *Nano Energy*, 2017, **39**, 444–453.

24 I. H. Kwak, H. S. Im, D. M. Jang, Y. W. Kim, K. Park, Y. R. Lim, E. H. Cha and J. Park, *ACS Appl. Mater. Interfaces*, 2016, **8**, 5327–5334.

25 C. C. L. McCrory, S. Jung, I. M. Ferrer, S. M. Chatman, J. C. Peters and T. F. Jaramillo, J. Am. Chem. Soc., 2015, **137**, 4347–4357

26 C. C. L. Mccrory, S. Jung, J. C. Peters and T. F. Jaramillo, *J. Am. Chem. Soc*., 2013, **135**(45): 16977-16987.